Preprints of the 21st IFAC World Congress (Virtual)
Berlin, Germany, July 12-17, 2020

Frequency Response Based Multivariable Feedback Control Design for Transient RCCI Engine Operation

Jan Verhaegh * **Frank Kupper** * **Frank Willems** *,**

* *TNO Automotive, Powertrains Department, Helmond, The Netherlands (e-mail: {jan.verhaegh,frank.kupper}@tno.nl)*
** *Dept. of Mechanical Engineering, Eindhoven University of Technology, The Netherlands (e-mail: f.p.t.willems@tue.nl)*

Abstract: Reactivity Controlled Compression Ignition (RCCI) is a high efficient, pre-mixed combustion concept, which is characterized by controlled auto-ignition. RCCI control has to guarantee stable and safe operation for varying operating conditions. Research concentrated on next-cycle fuel path control, so far. However, a crucial step towards on-road implementation is accurate control of both air and fuel path, especially during transients. In this work, a systematic, frequency domain-based design method is presented for coordinated air-fuel path control. Starting from MIMO system identification using Frequency Response Functions, cylinder individual combustion models are developed. Based on these models, a static decoupling matrix and five SISO PI controllers are designed. The followed method allows to analyze and guarantee local robust stability, disturbance rejection and reference tracking properties. For transients, the controller is scheduled as a function of engine speed and torque. The potential of the designed MIMO controller is demonstrated on a six-cylinder Diesel-E85 RCCI engine. This controller shows good reference tracking for engine speed-load variations. Furthermore, it enables safe RCCI operation towards higher loads compared to open-loop control strategies.

Keywords: engine control, frequency response function, system identification, multivariable control, decoupling design, LPV control, experimental validation

1. INTRODUCTION

Reactivity Controlled Compression Ignition (RCCI) is an advanced combustion concept, which combines very high thermal efficiencies with ultra-low engine out pollutant emissions [Reitz, 2015]. This concept is characterized by in-cylinder blending of two fuels with different reactivities. This promotes the use of a wide range of (sustainable) fuels. Consequently, RCCI is a promising combustion concept for heavy-duty applications; it shows potential to realize dramatic CO_2 reduction levels as well as realizing near zero impact nitrogen oxides (NO_x) and particulate matter (PM) emission levels. These are essential features to realize green transport in the near future.

In order to bring the RCCI concept on the road, the main control challenge is to realize stable and safe operation under varying operating conditions. This pre-mixed combustion concept relies on controlled auto-ignition of a mixture of fuels, air, and combustion products from previous cycles. More precisely, fueling ends well before start of combustion, so it lacks direct control of the combustion process. RCCI is chemically controlled and is very sensitive to in-cylinder condition variations, e.g. in mixture composition and temperature. This is especially challenging for multi-cylinder applications, where the mixture of air, recirculated combustion products and upstream injected fuel is typically unevenly distributed over the cylinders. In addition, these conditions will change over time during dynamic engine operation, which corresponds to varying engine speed and load.

Closed-loop combustion control is essential to guarantee robust stability in pre-mixed combustion concepts [Willems, 2018]. RCCI is a relatively new research area and did not attract much attention from the control community so far. A few studies are only found in the open literature, which typically focus on combustion phasing control, see e.g. [Olsson, 2001; Hanson, 2004; Strandh, 2004; Arora, 2017]. In these studies, next cycle fuel path control is applied to realize the desired combustion phasing (CA50) or Indicated Mean Effective Pressure (IMEP), which is a measure for engine load. In all cases, PID controllers are applied, which are manually tuned. [Strandh, 2004] compared a CA50 PID and LQG controller on a six cylinder engine. For this SISO case, good reference tracking and disturbance properties are found during engine speed and load steps. As shown in [Maurya, 2013; Willems, 2019], strong input-output coupling is encountered in the MIMO case. However, a systematic control design approach that deals with coupling and that guarantees stability and robustness is missing. All cases focus on fuel path control only, but coordinated air-fuel path control is key to realize the desired in-cylinder conditions. This especially holds for dynamic engine operation. For an overview of various RCCI control studies, the reader is referred to e.g. [Arora, 2017; Willems, 2019].

In this work, a systematic, frequency-based control design method is introduced for coordinated air-fuel path control. Focus is on the RCCI control problem, but this method can also be applied to other pre-mixed and conventional combustion concepts. We combine linear parameter-varying (LPV) static decoupling with loop shaping control design. In previous studies, we only focused on fuel path control in simulations [Indrajuana, 2016] and on results for an RCCI engine without exhaust gas recirculation (EGR valve was always closed) [Willems, 2019]. Compared to earlier work, the main contributions of this work are:

- **Control design method is presented in detail**; this includes frequency response function (FRF) system identification, system analysis and feedback control design using loop shaping;
- **EGR control valve is included** in MIMO control design;
- **New experimental results for a six-cylinder Diesel-E85 RCCI engine**, which demonstrate the potential of the new MIMO controller for relatively fast load ramps.

This paper is organized as follows. First, the studied experimental set-up and the associated control problem are defined in Section 2 and 3, respectively. Section 4 introduces the followed systematic design approach in detail. Then, the experimental results are presented and discussed in Section 5. Finally, the main conclusions are summarized and directions for future work are suggested.

2. EXPERIMENTAL SETUP

The studied engine platform is based on a modern six cylinder EURO-VI Diesel engine. It is equipped with a common rail fuel injection system and a cooled, high pressure EGR system. For advanced RCCI experiments, the following hardware has been installed, see Fig. 1:

- Port fuel injection (PFI) system;
- Modified piston with compression ratio 15:1;
- Modified turbocharger with a Variable Geometry Turbine (VGT);
- Pressure sensor in each cylinder.

The engine runs on Diesel (EN590) and E85 during all experiments.

2.1 Data Acquisition

The RCCI engine is equipped with standard temperature, pressure, mass flow and rotational speed sensors at various locations. Tailpipe emissions are measured using a Horiba MEXA ONE unit. All emission signals are logged at 10 Hz by the STARS automation system. For combustion analysis, Kistler 6125C pressure sensors are installed in each cylinder. Together with crank angle information from an AVL 365x pulse system, this cylinder pressure data is processed using an AVL Indimodul 621.

2.2 Real-time Control System

For real-time combustion control, a Speedgoat target computer is used, as shown in Fig. 1. This hardware platform consists of an Intel Core i7 3.5 GHz CPU and a Kintex

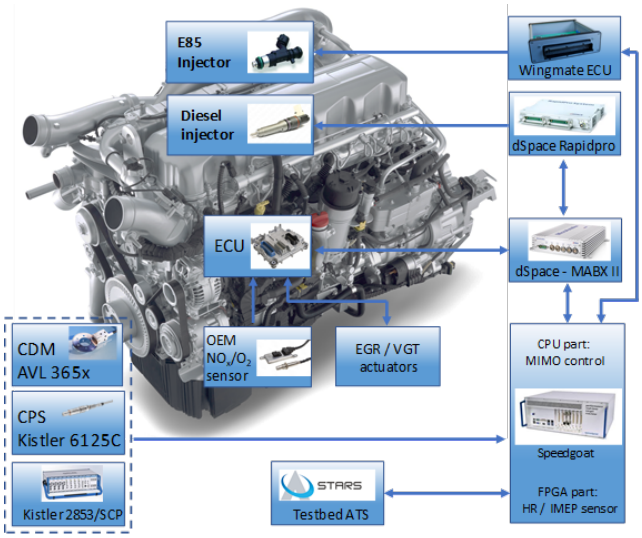

Fig. 1. Six-cylinder RCCI engine with dedicated, real-time control system [Willems, 2019].

7 FPGA. The FPGA part processes the analogue in-cylinder pressure signals, and updates the cylinder individual combustion phasing (CA50) and net Indicated Mean Effective Pressure (IMEPn) during each combustion cycle. The Simulink control software runs in the CPU part and operates at a sample frequency of $f_s = 100$ Hz. The Speedgoat system sends its desired control actions to: i) Wingmate ECU, which controls the E85 PFI fuel injection, and ii) dSPACE MABXII, which controls the VGT and EGR valve position and the diesel injection for the individual cylinders.

2.3 Engine Operating Points

This experimental study focuses on three engine operating points: (A) high-way driving, (B) engine load increase, and (C) engine speed increase. The corresponding actuator settings and operating conditions are listed in Tab. 1.

Table 1. Nominal RCCI operating conditions.

Parameter	Unit	Operating Point		
		A	B	C
Engine speed ω_e	rpm	1000	1000	1300
IMEPn	bar	8.5	11.5	8.5
Energy-based blend ratio	%	81.8	87.0	78.6
Air Fuel ratio λ_{AF}	-	2.3	2.2	2.5
Intake manifold pressure	bar	1.98	2.40	2.05
Intake manifold temp.	°C	32.5	34.0	32.0
VGT position u_{VGT}	% open	38	35	56
EGR position u_{EGR}	% open	20	20	20
Diesel inj. tim. $u_{\mathrm{SOI\ Diesel}}$	°CA aTDC	-40	-42	-40
Diesel rail pressure	bar	500	500	500
Diesel DI quantity u_{QDiesel}	mg/inj	20.5	18.0	23.0
E85 PFI quantity u_{QE85}	mg/inj	136	180	125

The selected settings are derived from multiple engine parameter sweeps. They result from finding a trade off between high thermal efficiency and low engine out emissions within the constraints set by stable and safe operation. For more information on the engine sweeps, we refer to the results in [Willems, 2019].

3. RCCI CONTROL

Before discussing the proposed RCCI control system architecture, this section starts with the definition of the RCCI control problem. Then, the feedforward and feedback controller are presented.

3.1 RCCI Control Problem

Fig. 2 shows the RCCI engine with its control system. The RCCI engine controller has to realize the requested engine power with maximal brake thermal efficiency while meeting emissions, safety and noise constraints. To avoid engine damage, the peak in-cylinder pressure (PMAX) and peak in-cylinder pressure rise rate (PPR) are limited. The later parameter is also associated with noise. These high level control objectives are indicated by z. During real-world operation, this has to be achieved under various external disturbances w, such as different duty cycles, ambient conditions and fuel composition, and under plant uncertainty (e.g. production tolerances and component aging).

For RCCI combustion, the main control challenge is to guarantee robust stability. This pre-mixed combustion concept relies on auto-ignition of a mixture of fuels, air, and combustion products from previous cycles. As this process is chemically controlled, it is very sensitive to variations in operating conditions. Uncontrolled combustion can result in knocking, high peak cylinder pressures at high load and misfires or partial combustion at low load. This has to be avoided, since it can result in engine damage, unacceptable noise levels and high CO and HC emissions, respectively.

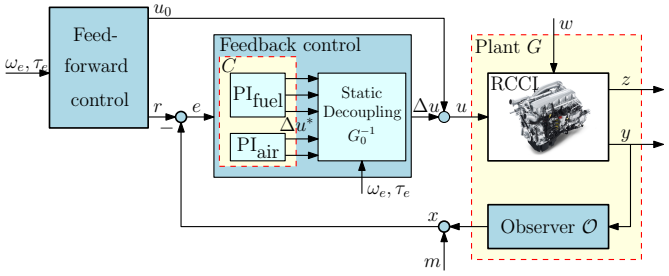

Fig. 2. RCCI engine with the proposed control system architecture, similar to [Willems, 2019].

3.2 RCCI Control Architecture

Fig. 2 shows the proposed RCCI control architecture: a combination of a feedforward and feedback controller. The objective of the feedforward controller is to achieve nominal optimal performance, while the feedback controller has to guarantee robust performance using real-time information from the observer $\mathcal{O}$ (also called virtual sensor). For combustion control, cylinder individual IMEPn and heat release are estimated for each combustion cycle using in-cylinder pressure information. Details about the implemented virtual sensors can be found in e.g. [Willems, 2018]. Both controllers are discussed in more detail below.

3.3 Feedforward Controller

Based-on engine speed ω_e and requested engine torque τ_e, the feedforward controller determines the nominal actuator settings u_0 and the corresponding reference r for the feedback controller, as illustrated in Fig. 2. In the studied setup, the following control inputs are available:

$$u = \left[u^i_{\text{QE85}} \;\; u^i_{\text{QDiesel}} \;\; u^i_{\text{SOI Diesel}} \middle| u_{\text{VGT}} \;\; u_{\text{EGR}} \right]^\top, \quad (1)$$

with E85 quantity u^i_{QE85} in mg/inj, diesel quantity u^i_{QDiesel} in mg/inj, diesel injection timing $u^i_{\text{SOI Diesel}}$ in deg CA aTDC, VGT position u_{VGT} in %, and EGR valve position u_{EGR} in %. Note that we have cylinder individual fueling capability, which is indicated by the cylinder number $i = \{1, 2, \ldots, 6\}$.

Typically, the high-level objectives z cannot be observed directly on production engines. With the introduction of cylinder pressure sensors, new options become available: for each combustion cycle, e.g., net indicated thermal efficiency and NO emission can be determined [Willems, 2018]. However, this still requires an accurate estimate of combustion efficiency and correlations, respectively. Also, for brake thermal efficiency and brake specific emissions (in g/kWh), estimated friction losses have to be available. Therefore, based on correlations $z(x)$ and on their controllability, the following reference signals r are selected:

- **Net Indicated Mean Effective Pressure** (IMEPn) is a cylinder individual measure for engine load and is an indicator for misfires and partial combustion;
- **Energy-based blend-ratio** is defined as:
$$\text{BR} = \frac{\dot{m}_{\text{E85}} \text{LHV}_{\text{E85}}}{\dot{m}_{\text{E85}} \text{LHV}_{\text{E85}} + \dot{m}_{\text{diesel}} \text{LHV}_{\text{diesel}}} \cdot 100\%, \quad (2)$$
where $\dot{m}$ denotes the mass flow and LHV the lower heating value. It has a strong link with HC and CO emissions and combustion stability;
- **Combustion phasing** (CA50): expressed as the crank angle where 50% of the total heat is released. It is an important indicator for the mixing period and for combustion stability. Also, CA50 is closely linked to thermal efficiency;
- **Exhaust manifold pressure** p_{em} is associated with EGR mass flow and pumping losses;
- **EGR ratio** is given by:
$$\text{EGR ratio} = \frac{\dot{m}_{\text{EGR}}}{\dot{m}_{\text{EGR}} + \dot{m}_c} \cdot 100\%, \quad (3)$$
with EGR mass flow $\dot{m}_{\text{EGR}}$ and compressor fresh air flow $\dot{m}_c$. It is a measure for the EGR flow and is linked to the oxygen content in the intake manifold.

Note that the selected set of controlled variables is the result of a careful balance between performance and combustion stability considerations.

During transient conditions, the feedforward controller linearly interpolates between the calibrated values in the 2D look-up tables $u_0(\omega_e, \tau_e)$ and $r(\omega_e, \tau_e)$.

3.4 Feedback Controller

The feedback controller aims to: i) track the desired reference values r, ii) guarantee robust performance with respect to system uncertainties ΔG , and iii) reject external

disturbances, including measurement noise m. Assuming that the static decoupling is effective, the fuel and air path feedback control loops are treated independently. Consequently, we implement the following diagonal multi-variable controller:

$$C = \left[\begin{array}{ccc|cc} c_{\text{IMEPn}} & 0 & 0 & 0 & 0 \\ 0 & c_{\text{BR}} & 0 & 0 & 0 \\ 0 & 0 & c_{\text{CA50}} & 0 & 0 \\ \hline 0 & 0 & 0 & c_{\text{pem}} & 0 \\ 0 & 0 & 0 & 0 & c_{\text{EGR ratio}} \end{array}\right]. \quad (4)$$

Next-cycle fuel path control Combustion phasing and heat release control are key for stable and safe RCCI combustion. Next-cycle PI control is applied for $c_{\text{IMEPn}}, c_{\text{BR}}$ and c_{CA50} using forward Euler integration:

$$\Delta u[k] = K_P e[k] + (K_I T_{\text{cycle}} - K_P)\, e[k-1], \quad (5)$$

where $e[k] = r[k] - x[k]$ for combustion cycle k, and T_{cycle} is the combustion cycle time. For ease of implementation, the three SISO feedback controllers have identical control parameters K_P and K_I for the individual cylinders. Therefore, the superscript i is omitted in Eq. (4). Potential cylinder-to-cylinder differences are dealt with in the control design. It is noted that the (variable) update frequency of the next-cycle fuel path controller is set by the engine speed ω_e (in rpm). For $\omega_e = 1000$ rpm, this results in $T_{\text{cycle}} = 0.12$ seconds. In addition, the compensation Δu will be held for one combustion cycle, i.e. T_{cycle} seconds. This effect can be interpreted as zero-order hold (ZOH) behavior. In this work, the feedback control design approach is done in the continuous-time domain. However, we will keep in mind that the fuel-path feedback controller is actually implemented in a discrete-time event-based way [Åström, 1990].

Air path control The two SISO PI controllers are running in the time domain and operate with an update frequency of f_s. Typically, the dynamics of the air path are slower than the dynamics of the fuel path. This limits the maximum closed-loop bandwidth of the air path controllers.

4. FREQUENCY-BASED CONTROL DESIGN

For the design of the engine feedback controller, a frequency domain-based approach is followed. Three important steps can be distinguished in this approach:

(1) MIMO system identification using Frequency Response Functions (FRF);
(2) Static decoupling design;
(3) Loop shaping of parallel SISO controllers.

In the sequel of this section, these steps are discussed in detail for the design of the MIMO engine controller.

4.1 System Identification

Following [Pintelon, 2001], multi-sine excitation signals are applied to each individual input u to determine Frequency Response Functions (FRFs). This results in a square transfer function matrix for the studied multiple-input multiple-output (MIMO) system:

$$G(j\omega) = \frac{X(j\omega)}{U(j\omega)} = \left[\begin{array}{c|c} G^i_{\text{inj-comb}} & G^i_{\text{valves-comb}} \\ \hline G_{\text{inj-air}} & G_{\text{valves-air}} \end{array}\right]. \quad (6)$$

This is a linear model of the RCCI engine with observer $\mathcal{O}$ around the engine operating point (ω_e, τ_e) with input u according to (1) and observed outputs:

$$x^i = \left[\, x^i_{\text{IMEPn}} \;\; x^i_{\text{BR}} \;\; x^i_{\text{CA50}} \,\middle|\, x_{\text{pem}} \;\; x_{\text{EGR ratio}} \,\right]^\top. \quad (7)$$

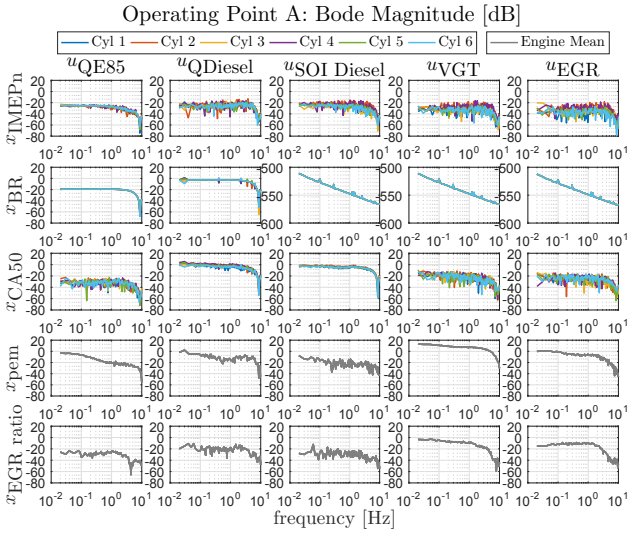

Fig. 3. FRF results for operating point A.

For a multi-sine excitation of 800 seconds (zero-mean, random phase), the results are shown in Fig. 3. As RCCI engines rely on controlled auto-ignition and are sensitive for operating conditions, caution is necessary during the design of these excitation signals. Nominal operating conditions are selected with sufficient margin to the unstable operating range. Also, small but sufficient amplitudes of the excitation signal are chosen, such that safe operation with acceptable signal-to-noise ratios is guaranteed. Excitation frequencies are chosen between 0.02 Hz and 10 Hz. The FRFs do not only capture the engine and observer behavior, but they also identify actuator and sensor dynamics. Moreover, the behavior of the individual cylinders $G^i_{\text{inj-comb}}$ and $G^i_{\text{valves-comb}}$ is determined, as illustrated in the upper part of this figure.

In this study, we focus on cylinder-averaged behavior, such that we can apply one feedback control parametrization to all six individual cylinders. This simplifies the control implementation. Therefore, the superscript i is omitted in the sequel.

4.2 Static Decoupling Design

Using the low-frequent part of G in Fig. 3, a static decoupling matrix G_0^{-1} is designed, such that the multiplication $\bar{G} = GG_0^{-1} \approx I$ for low enough frequencies. The matrix G_0^{-1} is effectively realizing the decoupling of the air and fuel path. Note that an unique G_0^{-1} is derived for each operating point A, B and C. During transient engine operation, the entries of the (local) static decoupling matrix G_0^{-1} are scheduled as a function of ω_e and τ_e, see Fig. 2.

From an analysis of the Relative Gain Array (RGA) [Skogestad, 2015], it is concluded that the static decoupling is successful for frequencies up to 0.4 Hz.

4.3 Loop Shaping

Assuming that the system $\bar{G}$ is decoupled, the MIMO control design reduces to the design of five independent SISO feedback controllers, see Eq. (4). For these SISO systems, two steps are distinguished in the control design:

(1) **Transfer function approximation** of the diagonal terms of the decoupled system $\bar{G}$, i.e., for the diagonal terms $\bar{g}_{jj}$ with $j = \{1, 2, \ldots, 5\}$;
(2) **PI controller design** using frequency-domain loop-shaping for the loop gain $l_{jj} = \bar{g}_{jj} c_j$. In this step, we deal with requirements related to closed-loop stability, robustness and measurement noise rejection.

To illustrate this approach, the design of the controller c_{IMEPn} is discussed in detail.

Transfer function approximation Fig. 4 shows the FRF results of $\bar{g}_{11}(j\omega)$ for six individual cylinders. The behavior of cylinder 1 is approximated by a continuous-time transfer function, which is indicated by the black dashed line:

$$\tilde{g}_{11}(s) = \text{ZOH}(s) F(s), \tag{8}$$

with

$$\text{ZOH}(s) = \frac{1 - e^{-T_{\text{cycle}} s}}{T_{\text{cycle}} s}, \quad F(s) = \frac{6.745}{s + 6.745} e^{-0.12 s}. \tag{9}$$

This model consists of a zero-order-hold model ZOH(s) due to the cycle-based control updates, as explained in Section 3. The combustion physics $F(s)$ are approximated by a first-order model and an input delay of 0.12 seconds.

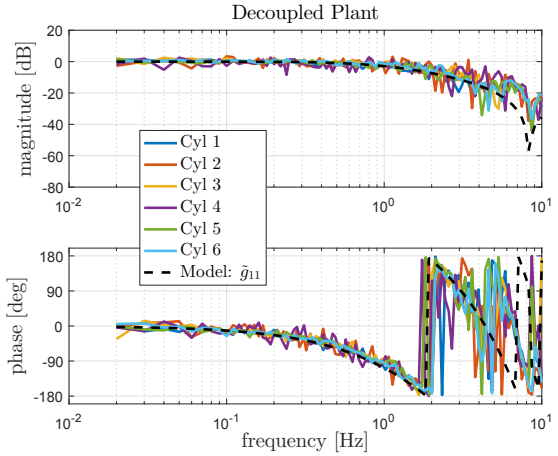

Fig. 4. FRF results of $\bar{g}_{11}(j\omega)$ for six individual cylinders (Operating point A).

SISO controller design In this study, SISO controllers are applied:

$$c_{\text{IMEPn}}(s) = \frac{K_P s + K_I}{s}. \tag{10}$$

For the air path controllers, a first order low-pass filter with cut-off frequency $1/(2\pi\tau)$ is added to filter out high-frequent measurement noise. Based on the transfer function estimate $\tilde{g}_{11}$, this controller is designed using the frequency-domain loop shaping method. More precisely, the loop gain $l_{11}(j\omega) = \tilde{g}_{11}(j\omega) c_{\text{IMEPn}}(j\omega)$ is shaped for closed-loop stability, while dealing with robustness margins and performance. The latter is expressed by the (bandwidth) cross-over frequency ω_{co} of the open-loop l_{11}. For robust performance, Gain Margin (GM), Phase Margin (PM) and Modulus Margin (MM) are considered, as defined by [Skogestad, 2015].

In order to deal with the cylinder-to-cylinder variations, the following target values have been set to guarantee robust performance: GM $>$ 6 dB, PM $>$ 30 deg and MM $<$ 6 dB. The applied PI control settings are listed in Tab. 2. Note that these settings are identical for all three operating points. For operating point A, the resulting robustness margins can be found in Tab. 3. Fig. 5 shows the corresponding Nyquist plot of l_{11} for the six individual cylinders. This figure illustrates that the robustness margins are respected.

Table 2. Settings for SISO fuel- and air-path controller for the three operating points.

SISO controller	K_P	K_I	τ
c_{IMEPn}	0.25	2.00	n/a
c_{BR}	0.25	2.00	n/a
c_{CA50}	0.25	2.00	n/a
c_{pem}	0.5	0.79	0.0159
$c_{\text{EGR ratio}}$	0.5	0.79	0.0159

Table 3. SISO performance indicators and robustness margins of feedback controller C for operating point A.

Output	Resp. time [cycles]	ω_{co} [Hz]	PM [deg]	GM [dB]	MM [dB]
x_{IMEPn}	8	0.27	86.5	14.5	2.5
x_{BR}	11	0.32	97.8	inf	0.5
x_{CA50}	9	0.26	77.2	15.6	1.6
x_{pem}	26	0.10	76.5	13.6	2.1
$x_{\text{EGR ratio}}$	32	0.11	94.1	6.4	5.6

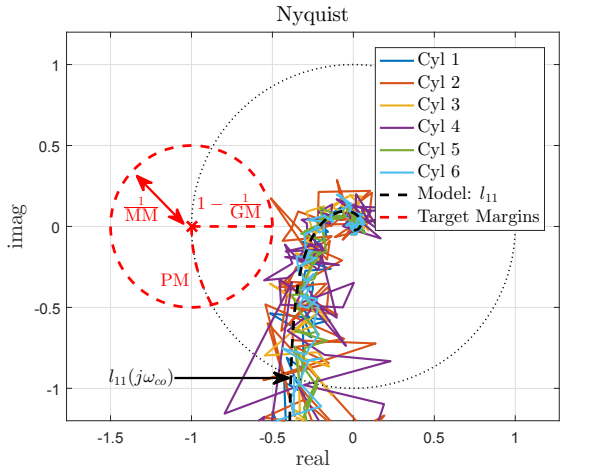

Fig. 5. Nyquist plot of l_{11} for six individual cylinders (Operating point A).

Besides robust stability, also rejection of measurement noise m and the response time is important. The sensitivity function directly shows the effect of m on the controlled

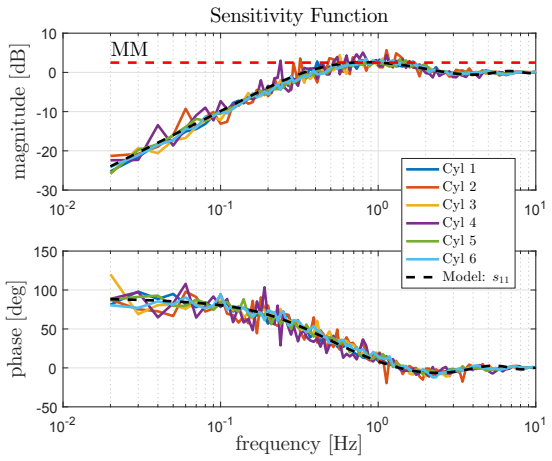

Fig. 6. Sensitivity function of measurement noise m_{11} to output x_{IMEPn} for the six individual cylinders.

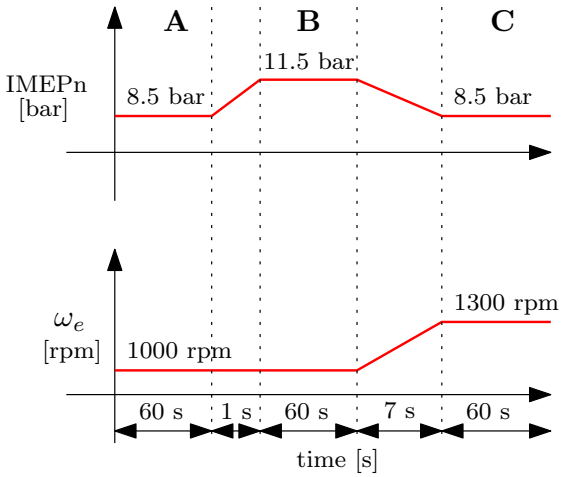

Fig. 7. Test procedure for transient performance evaluation of RCCI engine with MIMO controller.

output x. For $s_{11}(j\omega) = \frac{x_{\text{IMEPn}}}{m_{11}}$, the result is shown in Fig. 6. From this figure, it is seen that the designed feedback controller amplifies noise for frequencies above 0.27 Hz. The largest noise amplification is by a factor 1.33 (MM = 2.5 dB).

Tracking performance of a feedback controller is typically specified in terms of tracking error and response time. Here, the closed-loop response time is defined as the number of cycles needed by the output x to reach 90% of the reference input step r. As seen from Tab. 3, an increase of 1 bar in IMEPn is realized in 8 cycles. Also, the other combustion related parameters can be controlled relatively fast. However, due to air path dynamics, the response times for x_{pem} and $x_{\text{EGR ratio}}$ are approximately three times larger.

5. EXPERIMENTAL RESULTS

In this section, experimental results are presented for the RCCI engine with MIMO controller. First, the performance is analyzed around the stationary point A. Focus is on cylinder balancing and the reduction of cycle-to-cycle variations. Moreover, effective decoupling and reference tracking is examined. Second, the transient performance of the closed-loop controlled system is studied for the engine speed and torque changes shown in Fig. 7. More precisely, the studied operating points listed in Tab. 1 are connected via ramps. For this test case, a comparison is made between open-loop and closed-loop control performance.

5.1 RCCI Performance in Stationary Point

Cylinder balancing Cylinder balancing in a stationary point is demonstrated for operating point A. The RCCI setup is initially running with feedforward control u_0 only, i.e., no feedback control is applied ($\Delta u = 0$). In this open-loop control mode, all cylinders have identical nominal fueling settings, see Fig. 8. We observe significant cylinder-to-cylinder variations in combustion phasing x_{CA50} and x_{IMEPn}. The feedback controller C is switched on at engine cycle 139. As a result, the observed values x are controlled to their reference values r. As illustrated in Fig. 8, this results in different fuelling settings for the individual cylinders. This is mainly attributed to different injector behavior; although all injectors are calibrated, actual performance varies over time. In addition, EGR and λ distribution will not be equal over the six cylinders, which also affects the combustion process.

Moreover, the performance variables z_{PMAX} and z_{PPR} are also reduced for most cylinders. At the same time, we observe lower engine out NO_x emissions, but increased engine out THC emissions.

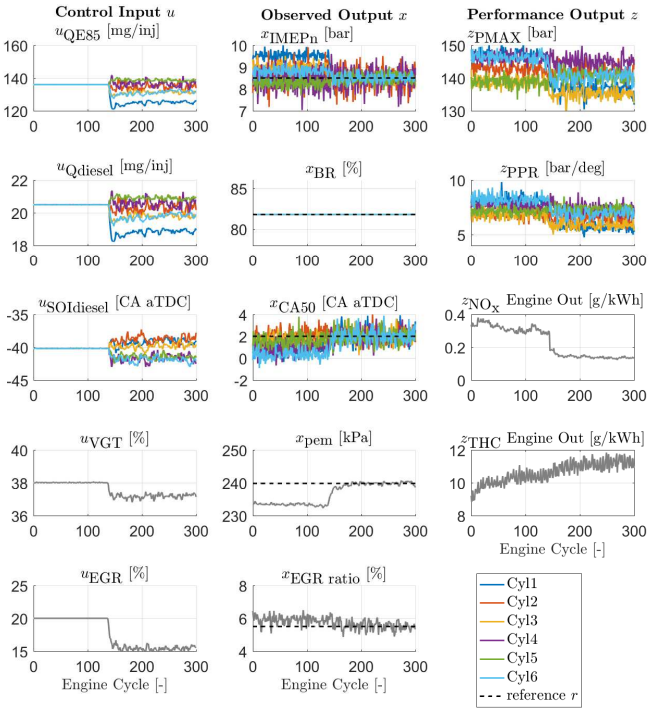

Fig. 8. Cylinder balancing in operating point A.

Cycle-to-cycle variations To analyze the cycle-to-cycle variance of IMEPn per individual cylinder i, here the following definition is used:

$$\sigma^2_{x^i_{\text{IMEPn}}} = \frac{1}{N}\sum_{k=1}^{N}(x^i_{\text{IMEPn}}[k] - \mu_{x^i_{\text{IMEPn}}})^2, \qquad (11)$$

where $x^i_{\text{IMEPn}}[k]$ is the IMEPn at cycle number k, and $\mu_{x^i_{\text{IMEPn}}}$ is the mean IMEPn for cylinder i over $N = 100$ cycles. Using a similar relation for CA50, the results in Tab. 4 are found. For IMEPn, the cycle-to-cycle variances are approximately the same for the open-loop and closed-loop mode. However, the cycle-to-cycle variances in CA50 are slightly increased in the closed-loop control mode.

Cylinder-to-cylinder variations The (mean) cylinder-to-cylinder variance for IMEPn is given by:

$$\sigma^2_{\text{IMEPn}} = \frac{1}{N}\sum_{k=1}^{N}\left(\frac{1}{6}\sum_{i=1}^{6}(x^i_{\text{IMEPn}}[k] - \mu_{\text{IMEPn}}[k])^2\right), \tag{12}$$

where $N = 100$ is the number of engine cycles and μ_{IMEPn} is the mean IMEPn value for all six cylinders at cycle k. From Tab. 5, it is concluded that the intra-cylinder differences in both CA50 and IMEPn are reduced significantly by closed-loop control.

Table 4. Cycle-to-cycle variance for the individual cylinders.

	IMEPn: $\sigma^2_{x^i_{\text{IMEPn}}}$ [bar^2]					
Mode	Cyl 1	Cyl 2	Cyl 3	Cyl 4	Cyl 5	Cyl 6
Open-loop	0.031	0.238	0.047	0.220	0.042	0.042
Closed-loop	0.036	0.185	0.040	0.201	0.050	0.030
	CA50: $\sigma^2_{x^i_{\text{CA50}}}$ [CA aTDC^2]					
Mode	Cyl 1	Cyl 2	Cyl 3	Cyl 4	Cyl 5	Cyl 6
Open-loop	0.242	0.297	0.220	0.363	0.336	0.206
Closed-loop	0.365	0.319	0.288	0.391	0.371	0.323

Table 5. Cylinder-to-cylinder variance.

Mode	**IMEPn:** σ^2_{IMEPn} [bar^2]	**CA50:** σ^2_{CA50} [CA aTDC^2]
Open-loop	0.302	0.680
Closed-loop	0.089	0.342

Input-output decoupling For the individual control loops, step wise changes are applied sequentially to the individual references r, see Fig. 9. As illustrated by the results in the middle figures, these signals r are tracked without affecting the other observed outputs x. This illustrates the successful input-output decoupling. This requires coordination of all control inputs u, as shown in the left-hand figures. The corresponding z_{PMAX} and z_{PPR} stay within their limits for safe operation: 200 bar and 20 bar/deg, respectively. From the step responses in Fig. 9, we determine a response time of approximately 10 cycles for IMEPn, 15 cycles for BR, 13 cycles for CA50, 25 cycles for p_{em} and 31 cycles for EGR ratio. These values are in line with the design values, which are listed in Tab. 3.

5.2 Transient RCCI Performance

Using the test procedure shown in Fig. 7, the transient performance of the designed RCCI controller is evaluated. In Fig. 10, the open-loop behavior, i.e. feedforward only, is compared with the closed-loop behavior (with feedback). In this figure, the mean cylinder behavior has been plotted in order to keep results readable. Note that still individual

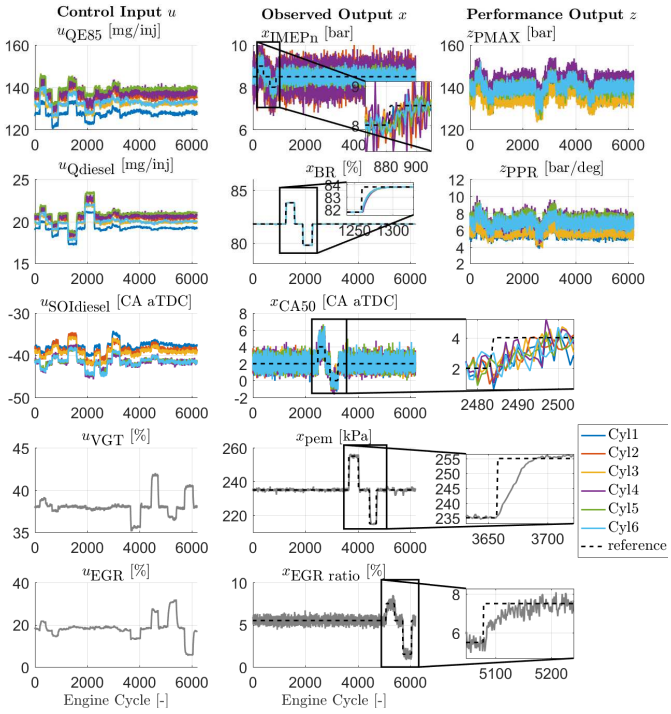

Fig. 9. Reference tracking around operating point A.

cylinder control has been applied. It is concluded that closed-loop control results in good tracking behavior for all five observed outputs x: in stationary operating points as well as during a change in engine load or engine speed.

For the open-loop CA50 response, a significant error is observed, which starts right after the load step at around 500 cycles. Over time, it slowly converges towards the set point value. This is due to engine heat up associated with the increased load and which makes the combustion start to advance. This CA50 drift indicates that the RCCI process is very sensitive to disturbances, such as temperature fluctuations. The closed-loop CA50 response shows the same initial error at the load increase as the open-loop case, because both rely on the same feedforward values. However, after one cycle, the feedback control ensures that the observed CA50 converges towards the set point value within a few cycles.

Feedback control does not only eliminate drift in the observed outputs, it also significantly reduces drift of the performance outputs z. Due to improved robustness, smaller margins in safety and emission constraints can be used. These reduced margins can be exploited in calibration to achieve lower fuel consumption and a higher load range.

6. CONCLUSIONS

In this paper, we present a systematic, frequency response-based control design methodology for coordinated air-fuel path control in a RCCI engine. Contrary to earlier work, the EGR loop is also considered in the control design. The proposed MIMO control architecture combines static decoupling with a diagonal feedback controller. The developed control strategy is implemented on a six-

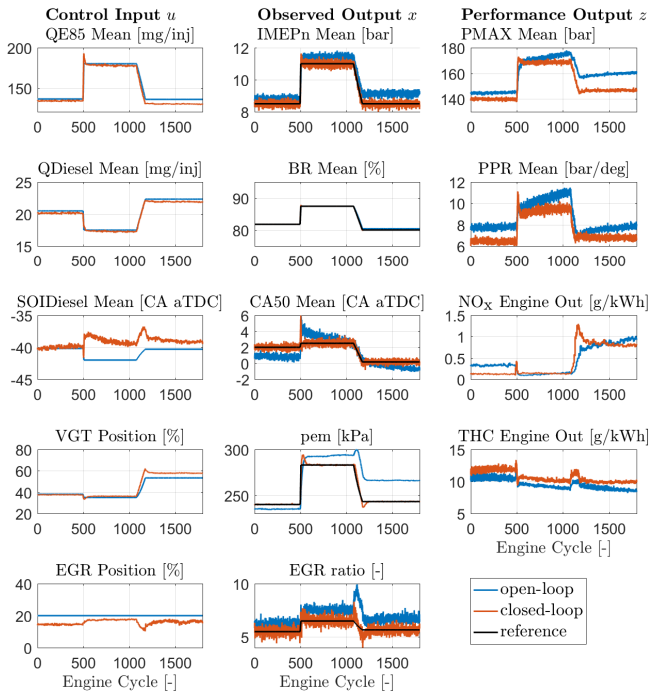

Fig. 10. Transient RCCI performance open-loop versus closed-loop for proposed test procedure.

cylinder Diesel-E85 RCCI engine. From this study, the following conclusions are drawn:

- **FRF system identification is an efficient method to determine cylinder individual models of the complex RCCI combustion process.** These data-driven models also capture sensor and actuator dynamics and open the route to model system uncertainty due to cylinder-to-cylinder variations;
- **The static decoupling matrix effectively decouples the original system up to frequencies of 0.4 Hz.** Using this result, the MIMO feedback control problem is reduced to the design of five parallel SISO controllers;
- **Five SISO PI controllers are designed with guaranteed (local) closed-loop stability and robustness margins** by following a frequency-based loop-shaping design procedure;
- **Functionality of the linear parameter-varying MIMO controller is successfully demonstrated on a six-cylinder RCCI engine**; effective input-output decoupling and reduction of cylinder-to-cylinder variations, especially for CA50. Moreover, good reference tracking of all controlled variables is shown for engine speed and load ramps;
- **Coordinated air-fuel path control enhances RCCI engine performance**: compared to the open-loop control case, PMAX and PPR are reduced, which enables safe RCCI operation at higher loads.

Future research will focus on advanced MIMO control design to further improve transient RCCI engine performance. As a next step, we plan to apply the Lyapunov-based design method of [Luo, 2018], which minimizes the stochastic cyclic variations and guarantees local closed-loop stability and dynamic performance specified by an upper bound on the tracking convergence rate. This method can also deal with model uncertainty. The potential of this method has to be demonstrated for speed-load changes as well as for real-world cycles.

REFERENCES

R.D. Reitz and G. Duraisamy. Review of high efficiency and clean Reactivity Controlled Compression Ignition (RCCI) combustion in internal combustion engines Progress in Energy and Combustion Science, vol. 46, pp. 12-71, 2015.

F. Willems Is cylinder pressure-based control required to meet future HD legislation? IFAC-PapersOnLine, 51(31), pp. 111-118, 2018.

J.-O. Olsson, P. Tunestal, and B. Johansson. Closed-loop control of an HCCI engine. SAE Technical Paper 2001-01-1031, 2001.

P. Strandh, J. Bengtsson, R. Johansson, P. Tunestal et al. Cycle-to-cycle Control of a Dual-Fual HCCI Engine SAE Technical Paper 2004-01-0941, 2004.

R. Hanson and R. Reitz, Transient RCCI Operation in a Light-Duty Multi-Cylinder Engine, SAE Int. J. Engines, 6(3):1694-1705, 2013.

R. Maurya and A. Agarwal Experimental Investigation of Closed-Loop Control of HCCI Engine Using Dual Fuel Approach, SAE Technical Paper 2013-01-1675, 2013.

J. Arora and M. Shahbakhti. Real-Time Closed-Loop Control of a Light-Duty RCCI Engine During Transient Operations SAE Technical Paper 2017-01-0767, 2017.

A. Indrajuana, C. Bekdemir, X. Luo and F. Willems. Robust Multivariable Feedback Control of Natural Gas-Diessel RCCI Combustion IFAC-PapersOnLine, 49(11), pp. 217-222, 2016.

F. Willems, F. Kupper, S. Ramesh, A. Indrajuana and E. Doosje. Coordinated Air-fuel Path Control in a Diesel-E85 RCCI Engine , SAE Technical Paper 2019-01-1175, 2019.

S. Skogestad and I. Postlethwaite. Multivariable Feedback Control: Analysis and Design , Wiley, West Sussex, UK, second edition, 2015.

R. Pintelon and J. Schoukens. System Identification: A Frequency Domain Approach IEEE Press, New York, New York, USA, 2001.

K.J. Åström and B. Wittenmark. Computer-Controlled Systems: Theory and Design. Prentice Hall, Englewood Cliffs, New Jersey, second edition, 1990.

X. Luo, M. Donkers, B. de Jager, and F. Willems. $\mathcal{H}_2$-Norm-Based Multi-Pulse Diesel Fuel Injection Control with Minimal Cyclic Combustion Variation IEEE Control Systems Letters, 2(3), pp. 307-312, 2018.